

Spatio-temporal climatic change of rainfall in East Java Indonesia

Edvin Aldrian^{a,b*} and Yudha Setiawan Djamil^a

^a Agency for the Assessment and Application of Technology, UPTHB - BPPT, Jl MH Thamrin 8, Jakarta, Indonesia

^b Marine Study Program, Faculty of Mathematics and Natural Science, University of Indonesia, Kampus FMIPA-UI, Depok, Indonesia

ABSTRACT: Spatial and temporal rainfall analysis of the Brantas Catchment Area (DAS Brantas), East Java, from 1955 to 2005 based on 40 rainfall stations with monthly rainfall data derived from daily rainfall data has been performed. To identify the climatic trend and annual changes in the area over the last five decades, we use the empirical orthogonal function (EOF) method based on multivariate statistics, followed by the fast Fourier transform (FFT) method for the power density spectrum analysis, the non-parametric Mann-Kendall trend test and the wavelet transform method. With EOF, we found the monsoonal rainfall pattern as the most dominant in this area, which explains about 72% of all variances. Without the annual signal, the leading EOF shows significant ENSO-modulated inter-annual and seasonal variabilities, especially during the second transitional period. We found a common and significant negative trend of accumulated rainfall and a negative trend of the monsoonal strength and dominance. This finding leads to changes in the annual pattern, which are increase in the ratio of rainfall during the wet season and increase of the dry spell period or the imbalance of the annual pattern. The increased ratio of the rainfall in the wet season has led to an increased threat of drought in the dry season and extreme weather in the wet season in recent decades. The role of the orographic effect had been detected from the decadal pattern, in which the high-altitude areas have greater rainfall amount all year round. From the decadal isohyets in December/January/February (DJF) and June/July/August (JJA), the rainfall amount decreased significantly during the last five decades as shown by a persistent increase of areas with low rainfall amount. By comparing the time series of rainfall data in two locations, the mountain and coastal areas, we discovered that the dry periods have increased, mainly in the low altitude area. Copyright © 2007 Royal Meteorological Society

KEY WORDS Indonesia; Java rainfall; climate trend; ENSO; decadal; EOF; wavelet

Received 9 June 2006; Revised 7 January 2007; Accepted 17 March 2007

1. Introduction

According to the intergovernmental panel on climate change (IPCC) report (IPCC, 2001), the surface temperature of the earth has risen steadily since the post-industry era of the 19th century. It is very likely that the observed global warming has contributed to a change in rainfall patterns on the local or regional scale. So far, no regional scale study has been performed over Indonesia to assess the possible interdependencies between the observed rainfall variability and climate trends over the last five decades. In their report, IPCC (2001) suggested that some model studies predicted a small change (below 5%) of rainfall over the Southeast Asian region as resulted from the inter-model consistency or no conclusive findings. Has the climate change in reality reduced or increased the rainfall over this region during past century or decades?. Such a question is very important nowadays, since during recent decades, pressure on demographic and population tension as well as agriculture and land cover change has put some areas of the world in water deficiency.

About the region, Suppiah and Hennessey (1998) and later Haylock and Nicholls (2000) have studied and reported an increasing trend of the Australian rainfall. The closest effort to this study for countries in Southeast Asia was made by Manton *et al.* (2001), who analysed trends of daily rainfall and temperature extremes of countries in Southeast Asia and Australia, including Indonesia. For the Indonesian region, they used six inadequate rainfall stations (Pangkal Pinang, Jakarta, Balikpapan, Manado, Ambon and Palu), from which they found no significant trend in any of the extreme rainfall indices in Indonesia. Moreover, for the entire region, they found that the number of rainy days (with at least 2 mm of rain) has decreased significantly throughout Southeast Asia and the western and central South Pacific, but increased in the north of French Polynesia and Fiji, and at some stations in Australia. Hence, to the authors' knowledge, there is no such study reported on climatic trend over local or regional maritime continent. Besides, spatial assessment of the climate impact and the trend is a relatively new topic for rainfall study in Indonesia.

While studies on the Indonesian rainfall regime date back to early 20th century (Braak, 1921), more detailed

* Correspondence to: Edvin Aldrian, BPP Teknologi (UPTHB), Jl MH Thamrin no 8, Lt 19, Jakarta 10340, Indonesia.
E-mail: edvin@webmail.bppt.go.id

studies on the Java rainfall were published long after that, for example, by Hackert and Hastenrath (1986), Konnen *et al.* (1998), Haylock and McBride (2001) and Aldrian and Susanto (2003). It is interesting to see the past changes of the rainfall pattern during the previous decades from the real observation data. One of the interesting local areas for such a study is the Brantas catchment in East Java province. The data from this area has been collected daily for quite a long time (more than five decades). With a good spatial and temporal coverage, this data is a valuable source of information of the local climatic changes that could be assessed. The result of this study will be useful in understanding the possible local impacts of the global climate change.

The Brantas catchment covers about 12 000 km² or about 35% area of the East Java Province (Figure 1). The total length of the main river is 320 km with the Brantas River itself being the second largest river in Java. The amount of annual average rainfall reaches 2300 mm (1991–2005 average) and about 80% of this falls during the wet season. Total potency of surface water reaches 12 billion m³, while the total dam capacity in the area reaches only 2.6–3 billion m³ yearly. The population of the Brantas basin was about 13.7 million in 1994, which is about 43.2% of the total population of East Java. The population density over the basin area is about 1.5 times the provincial average.

Considering the importance of the Brantas catchment area to the local and regional economy, a study of its long-term climatic trend is essential. The aim of this paper is the analysis of the spatial and temporal precipitation variability and trend in the Brantas catchment area, East Java, during the last five decades. Such a study is important for understanding the water potency at the surface and in the atmosphere. Changes in climatic

behaviour in recent decades temporally or spatially are important for the future projection of the water management. In this study, the time series of monthly precipitation data of 40 rain gauge stations between 1955 and 2005 were analysed. In order to achieve the objectives of the study, methods such as non-parametric tests, the wavelet method, the empirical orthogonal function (EOF) and spectral analysis were used. The study is limited to temporal analyses from monthly to decadal. The climatic factor for higher frequency from daily up to intra-seasonal will be disregarded in this study. In the following we will discuss the data and method of analyses followed by some of our results, discuss some topics related to previous results and, in the final section, conclude the highlights of our study.

2. Data and model

We used daily rainfall data from 40 rain gauge stations over the catchment area (07.2°S–08.4°S and from 111.5°E to 113.0°E; Figure 1). Those data are managed and collected by the Brantas catchment authority or Perum Jasa Tirta I. The analyses are conducted with regard to rainfall data of 51 years from 1955 to 2005. There are 27 rain gauges before and 26 rain gauges after 1991 used for this study. Among those are 13 stations with continuous data record over the entire analysis period. Thus, we have in total 40 rain gauge stations for this study. Moreover, since 1991, the local authority has modernized the data collection using an integrated automatic telemetry system.

Since we are dealing with the long-term climatic trend, we rearranged the daily data into monthly data. Before we changed the data format into monthly, we checked for missing data and data consistency with a homogeneity test. The homogeneity was detected using the Craddock test (Craddock, 1979) by comparing with the nearby stations. Among the different homogeneity tests described by Peterson *et al.* (1998), this method is the most feasible and easy to implement. Hence, we found a problem of data before and after 1991 in several stations. Before 1991, all rain gauge stations recorded manual data from each rain gauge taken once daily in the morning (around 00 UTC). Since the beginning of 1991, data have been recorded automatically; therefore the record will measure instantaneous data and not once daily like before 1991. With such different measurement methods, there was a consistency problem from data before and after 1991. The data before 1991 on several stations were adjusted according to the level of data after 1991 to preserve homogeneity of the monthly data. Also, we performed a gridding process of the rainfall data in the study area using the Cressman objective analysis (Cressman, 1959) gridding method to minimize the risk of missing data of one or a few stations. The grid system uses a spatial resolution 0.08° or about 8.9 km² and has 25 grid cells longitudinally and 15 grid cells latitudinally for our area of study. During the gridding process, about

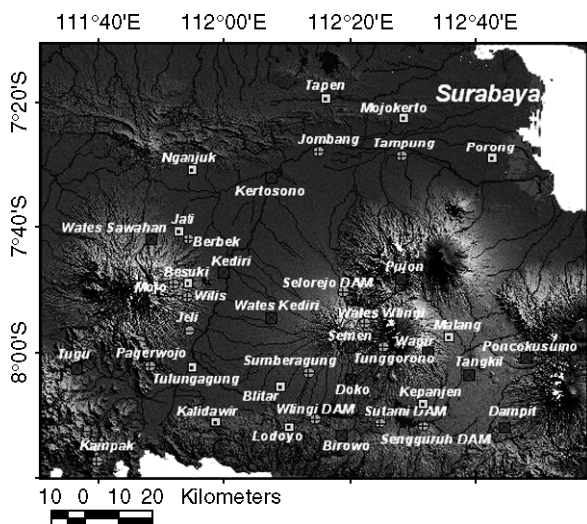


Figure 1. The Brantas river catchment area in East Java, Indonesia, where the rain gauge stations are located. The Brantas river starts near Tangkil, Malang and Poncokusumo, and then goes around the Arjuna and Kelud Mountains southward, westward and northward before it turns eastward and ends in two estuaries near Porong and Surabaya city.

0.18% of total grid cells were missing and we replaced them with their respective decadal monthly averages. Although the data period of each station is not the same, after the gridding process, we managed to fill all grid cells homogeneously for the period from January 1955 to December 2005. The latter condition is essential to run the EOF method (explained later); otherwise the EOF method will not work.

In this study, we use several trend analysis methods and focus on spatial trend analyses. Data from the stations were used for individual trend analysis using the non-parametric Mann–Kendall trend test and the spectral analyses of the wavelet transform. The rest of analyses were performed under gridded data for trend analyses using a combination of the EOF and the fast Fourier transform (FFT) methods.

The Mann–Kendall (Kendall, 1938; Mann, 1945; Kendall, 1970) test is a non-parametric test, which does not require the data to be distributed normally. But the time series used in this study have a normal distribution with some exceptions such as in the case of precipitation and the frequency of the circulation forms. The second advantage of the test is its low sensitivity to abrupt breaks due to an inhomogeneous time series. This test is used to analyse the statistical significance of all trends. Such a test will be performed on all trend analyses in this study to derive significant level and confidence on the trend analysis. This test is performed on stations with no location change during the last five decades, i.e. there are 13 stations for monthly as well as for annual rainfall trends.

The wavelet transform is an extension of the Fourier transform method or a running (windowed) FFT method, using a certain window size and sliding it along in time, computing the FFT at each time using only the data within the window. The wavelet analysis (Torrence and Compo, 1998) works furthermore by attempting to decompose a time series into time/frequency space simultaneously. One gets information on both the amplitude of any 'periodic' signals within the series, and how this amplitude varies with time. The method will calculate the power spectrum of the data series. The wavelet analysis is calculated using the Morlet mother wavelet for the power and global spectra. In this study, we are interested in the annual trend of rainfall, which is derived from information after using the wavelet analysis. The method was applied on all continuous station data, and then we calculated the linear trend as well as the corresponding statistical significance using the Mann–Kendall trend test.

In order to classify the climatic trend for the last five decades, we separate monthly data into decadal data of five groups, 1955–1964, 1965–1974, 1975–1984, 1985–1994 and 1995–2005 and one dataset covering the whole data 1955–2005 (inter-annual data). We will look at the isohyet (rainfall iso-contour) of each data group and compare it with the whole time series (inter-annual). Isohyets are spatial lines showing the same amount of rainfall in a certain area. Thus, we will have the average spatial pattern of each decade and

the total time series. After we classified data into their decadal groups and as a whole, we performed the EOF (Preisendorfer, 1988) and FFT (Press and Rybicki, 1989) analyses on each data group in order to obtain dominant spatial patterns as well as their long-time behaviour and frequency distributions of the principal components of the dominated spatial pattern, respectively. The EOFs are defined as the eigenvectors of the covariance matrix derived from the time series of the data field (von Storch, 1995; Wilks, 1995). The time series associated with the first EOF (PC) is investigated with respect to its temporal variability.

3. Results and analyses

3.1. Annual pattern and inter-decadal variability

The spatial rainfall pattern of the Brantas catchments area for the monthly average data clearly indicates the 1-year periodicity of the monsoonal pattern, with the maximum value occurring during the peak of the wet season from December to February. The amount of rainfall decreases to a minimum during the peak of the dry season from June to August. This pattern follows the Southeast Asian monsoonal wind pattern that also passes over the catchment, which brings moist air with high humidity from the South China Sea at the time of wet season, known locally as the *West Monsoon*. On the other hand, in dry season the wind brings dry air from the Australian continent in a period known locally as the *East Monsoon*.

The average annual rainfall pattern (1955–2005) as shown in Figure 2 clearly shows the monsoonal behaviour in the Brantas catchment area with high-intensity rainfall from October to April. By a definition from the Indonesian Bureau of Meteorology (BMG), an above-normal or wet month is declared when a 10-day period passes with a rainfall amount exceeding 50 mm or about 150 mm/month. Thus, we notice that November to April is considered as the wet season. Moreover, we also see that the rainfall contour follows the orography, as mountain areas always have a larger amount of rainfall than lowland areas. The high mountainous area seems to preserve a high rainfall amount all year round and even during the peak of the dry season. During the wet season, the mountainous areas receive more rainfall and, in fact, the increase of rainfall from the dry to the wet season over mountainous areas is more than those over lowland areas. The propagation of the wet area on the on-set of the wet season and its offset begin from the lowland or coastal area up to the mountainous area. Hence, the lowland, especially the coastal area, is more susceptible to dryness than the mountainous area. After looking at the annual spatial pattern, we were interested to see the spatial trend changes occur during the past five decades. Then we chose December/January/February (DJF) and June/July/August (JJA) as months representing the wet and the dry seasons, respectively.

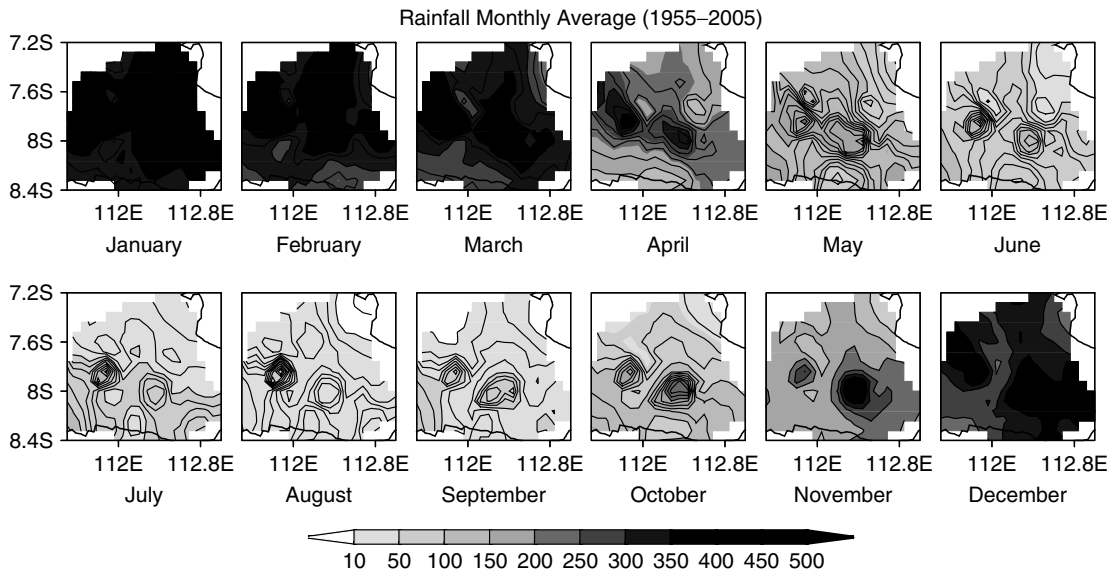


Figure 2. The annual rainfall pattern (mm/day) of the Brantas catchment area showing regular monsoon session that consists of dry and wet seasons.

The decadal spatial pattern changes as shown in Figure 3 illustrate a regular trend on certain months like DJF and JJA. Those spatial patterns show a greater expansion of the dry area in the later decades, which indicates the decrease of the yearly amount of rainfall for the last five decades. The pattern shows that such phenomena occur in the lowland as well as in the mountainous areas. Besides, the decrease happens during the dry as well as the wet period, but with a larger decrease in the lowland, as we observe that the mountain areas are still receiving a high amount of rainfall. Using a similar analysis as in the monthly basis, the strongest declining trend on a decadal scale occurs in December

and May (Table I). Thus, on the basis of the information of the last two paragraphs, we expect, in recent years, greater rainfall intensities over the mountains during the wet season and longer dry period over the lowland.

3.2. Individual station climatic trend

Before looking at the spatial analyses, we will investigate the trend of each station data using the Mann–Kendall trend test directly on monthly and annual data. Then the wavelet method will be used for comparison. Results of monthly and annual trend tests are given in Tables II and III, respectively. It is apparent from Table II that almost all stations have a decreasing trend except Semen,

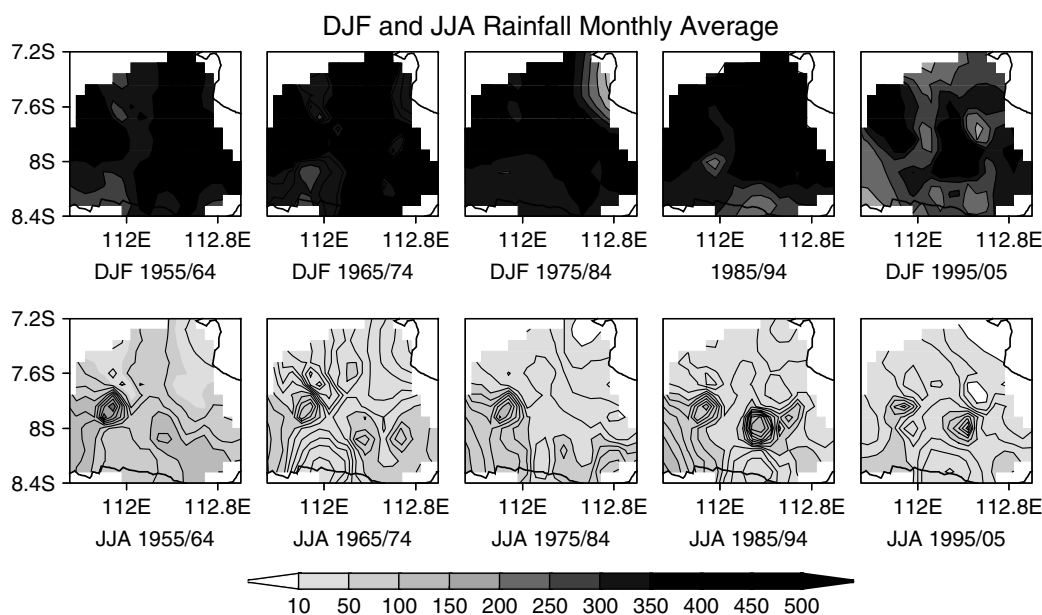


Figure 3. The decadal average changes of seasonal rainfall values in DJA and JJA as represented by the wet and dry seasons over the Brantas catchment area.

Table I. The decadal area average of seasonal and monthly trends (mm/month).

Period	1955–1964	1965–1974	1975–1984	1985–1994	1995–2005
DJF	368.00	369.94	360.26	386.79	299.12
JJA	81.22	44.66	50.52	50.04	35.56
December	359.87	327.67	320.13	326.42	268.36
May	154.47	175.20	148.30	86.81	76.12

which is located between two southern mountains and also receives shadow rainfall in dry and wet seasons. However, there is no supporting data from nearby stations that have similar characteristics. Moreover, most of the increase in trends are insignificant. On the other hand, Tangkil has the most significant decreasing trend. The trend during August is mostly undetected because of the inconsistent trend all over the study period and because of the large variability possibly from external forcings. Aldrian and Susanto (2003) classify this region as the southern monsoonal region, because it receives strong influences from large climate phenomena in the Pacific whose impact will be most pronounced in JJA. Furthermore, there is no significant trend during the transition period (August–November) between the dry and the wet season. On the contrary, many of significant values occur in March, April and May or the transitional period between the wet and dry period. The latter two facts indicate that the boreal spring transitional period (March to May) is more stable with a gradual and persistent decreasing trend than the other transitional period, which shows large inter-annual variability. The instability of trend from August to November indicates the possibility of the extension of the dry period to the second transitional period (extension of the dry spell period) than the extension of the wet period to the first transitional period: while for the first transition period there is no wet spell period but only a steady or stable

Table III. Linear regression of the long-term (51 years) annual rainfall trends. The linear regression was calculated according to the formula: $Annual\ rain = m \times year + b$. +, *, **, *** indicate Mann–Kendall significant levels of 0.1, 0.05, 0.01, 0.001, respectively.

Station name	Mann–Kendall		Linear regression	
	Z	Signific.	m (mm/year)	b (mm)
Tangkil	–3.90	***	–24.25	3072.68
Poncokusumo	–2.31	*	–15.44	2737.68
Wagir	–1.00	–	–6.92	2432.85
Birowo	–2.29	*	–17.62	2388.48
Wates Kediri	–2.59	**	–15.83	2479.50
Kediri	–2.58	**	–12.36	2336.37
Kertosono	–3.02	**	–16.94	2405.84
Tugu	–3.01	**	–21.79	2642.98
Dampit	–0.17	–	–1.23	2160.36
Doko	–1.64	–	–10.43	3316.45
Pujon	–2.52	*	–17.62	2576.87
Wates Sawahan	–2.47	*	–18.37	3176.00
Semen	0.71	–	6.48	3161.02

trend. Figure 4 illustrates what exactly occurs with the Tangkil station with the most significant monthly trends and explains the above hypothesis. On average, the largest decrease occurs in May followed by April or the boreal spring, and the lowest decrease in August, September and October.

Table II. The Mann–Kendall trend test Z-values for monthly rainfall, where the positive (negative) means an increase (decrease) in trend over 51 years. Underlined, bold and bold with a dark background represent significant levels at 0.1, 0.05 and 0.001, respectively. The Mann–Kendall trend test is not applicable to the same cases especially in August, where there is no consistent trend over the whole period.

Station name	Jan	Feb	Mar	Apr	May	Jun	Jul	Aug	Sep	Oct	Nov	Dec
Tangkil	–3.35	–1.85	–2.44	–1.33	–3.38	–1.17	–2.15	0.04	–1.16	–0.79	–0.80	<u>–1.92</u>
Poncokusumo	<u>–1.89</u>	–1.13	–1.41	–0.11	–2.91	–1.06	–1.56	–	0.38	–0.32	–0.22	–0.92
Wagir	0.18	–1.19	–0.45	–0.42	–1.34	0.43	–	–	1.05	–0.22	–0.41	–0.05
Birowo	–0.45	–0.83	–1.55	–1.31	–2.38	–1.43	–1.33	–	–0.50	0.40	–0.49	–2.36
Wates Kediri	–0.13	–0.51	–1.05	–0.67	–2.49	–1.00	<u>–1.86</u>	–	–1.22	–0.82	–1.07	<u>–1.74</u>
Kediri	–0.94	–0.71	–2.27	–0.82	–2.10	0.32	<u>–0.60</u>	–	–	0.43	–0.40	<u>–1.20</u>
Kertosono	–0.08	–1.59	–2.27	–1.42	–2.00	–0.61	–1.43	–	–	–0.63	0.11	–1.98
Tugu	–2.06	–0.76	–3.44	–1.04	–2.33	–0.46	<u>–1.73</u>	–1.51	–0.46	–0.40	–0.02	–1.18
Dampit	0.23	0.95	–0.50	0.18	–0.73	–0.11	0.04	–0.06	1.07	0.38	–0.04	–0.70
Doko	–0.17	–0.83	–0.63	–0.54	–1.59	0.05	–1.00	–1.45	–0.53	0.47	0.12	–0.44
Pujon	–0.71	–1.01	–2.32	–0.79	–2.36	–1.35	<u>–1.81</u>	–	–0.60	–1.39	–0.63	–1.05
Wates Sawahan	–0.38	–1.54	<u>–1.89</u>	–0.86	–2.76	–0.94	–	–	–	–0.15	0.00	–1.56
Semen	1.16	1.33	1.21	0.06	–1.14	<u>1.69</u>	0.58	–	0.41	0.70	0.91	0.60
Average	–0.66	–0.74	–1.46	–0.70	–2.12	–0.43	–0.99	–0.23	–0.12	–0.18	–0.23	–1.12

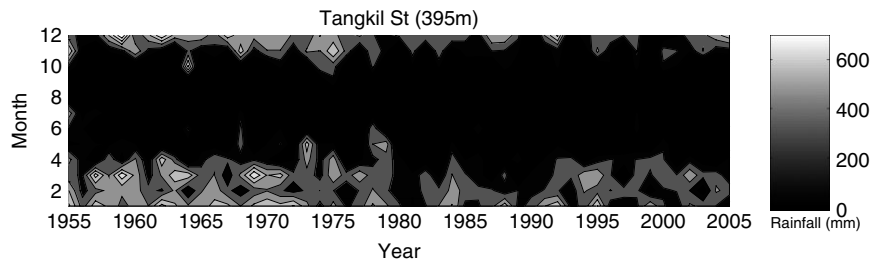


Figure 4. The monthly *versus* annual contour plot of Tangkil rainfall showing the stability of the boreal spring in contrast to the instability of the boreal fall. Therefore, the dry season, not the wet season, will be likely extended to the boreal fall transition period.

Similar analysis is applied for the total annual accumulated rainfall trend as shown in Table III. All stations except Semen have decreasing trends, and 9 out of 13 stations have significant level of their trends. Similar to the monthly trend analysis as in Table II, Tangkil has the most significant as well as the largest decrease among all stations, while Semen has an increasing trend, but the lowest decrease occurs in Dampit. However, this station, as well as Doko, has many missing data and therefore their results are quite unreliable. The decreasing trend of the annual rainfall will contribute to the total rainfall loss over the area. In the total 51-year period for the largest and the lowest decrease, there is an annual rainfall loss between 1236 and 62 mm, respectively, which is, for the largest, quite a substantial amount.

In this study we present another method for detecting climatic trend over the Brantas catchment using the wavelet method. The use of the wavelet method for detecting climate trend has been used in many studies. For example, Pisoft *et al.* (2004) used the inverse wavelet transform to calculate trends of the Czech temperature; Baliunas *et al.* (1997) to investigate trends in the central England temperature series; Park and Mann (2000) to detect shifts in global temperature and Datsenko *et al.* (2001) to analyse variability in European temperatures. Here we present a slightly different application to detect trend in the long-term rainfall data. From Figure 5 (right panel), the annual signal is the most pronounced one and in fact the only one above the threshold of 5% significance level. This means that, this area is dominated by the monsoonal signal. Thus, the trend analysis on the annual frequency will correspond to the most significant trends in the data, which is the monsoonal trend. Results of applying the wavelet method is tabulated in Table IV, with results quite similar to those from the direct application of the Mann–Kendall trend test. This method is different in the sense that we are only looking at the annual signal, while with the direct Mann–Kendall test we look at the total annual accumulation regardless of the frequency. The trend analysis using the wavelet method has a more significant level than its counterpart and has different stations with above-significant levels. One possible conjuncture for the latter phenomenon is our choice to analyse the annual frequency only.

3.3. The EOF–FFT analyses

The result of the EOF analyses for six data groups as defined above ('Data and Method' section) is given in Table V. From that table we notice the persistent dominance of the first eigen vector (eigen map), which always explains more than 64.8% of all variances or about ten times more than other eigen maps. From the power spectrum of the principal component data of each eigen map, we find that the first eigen map corresponds to the annual or the monsoonal pattern, which is the most dominant climate pattern. In fact, the power spectrum intensity from PC1 in the annual signal reaches about 6 times the second largest signal. The second and the third eigen maps do not seem to have any order of pattern according to the principal component and insignificant spectral intensities. The eigen map of the first pattern (PC1) of the inter-annual data in Figure 6 always shows positive values, which indicates that the whole Brantas basin has synchronized patterns to the monsoonal variability with some local differences between mountainous and lowland areas. Moreover, this eigen map contour follows the land morphology contour. The eigen values in the mountain areas are higher than

Table IV. The wavelet method indicators of the monsoon signal weakening. +, *, **, *** indicate Mann–Kendall significant level of 0.1, 0.05, 0.01, 0.001, respectively.

Station name	Linear regression gradient	Mann–Kendall Z	Mann–Kendall significant
Tangkil	−0.02597	−4.55	***
Poncokusumo	−0.01252	−2.75	**
Wagir	−0.00848	−1.56	–
Birowo	−0.01369	−2.18	*
Wates Kediri	−0.00923	−0.92	–
Kediri	−0.00610	−2.44	*
Kertosono	−0.01865	−3.89	***
Tugu	−0.02536	−3.72	***
Dampit	−0.03699	−0.19	–
Doko	−0.0006 ^a	−1.9	+
Pujon	−0.01457	−1.76	+
Wates Sawahan	−0.01467	−2.93	**
Semen	0.01068	1.28	

^a The results of Doko station is quite unreliable since there are too many missing data.

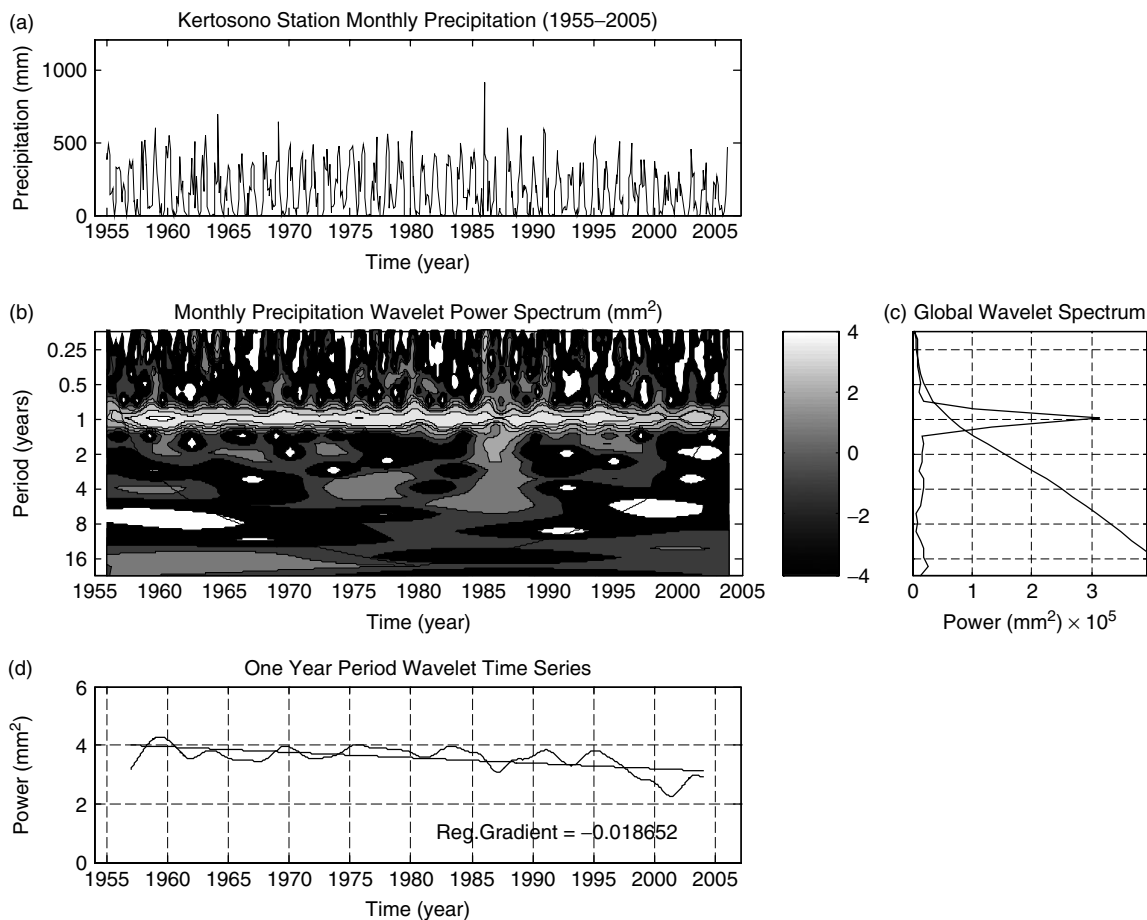


Figure 5. An example of the application of the wavelet method in detecting annual trend changes. Annual pattern has the most significant power spectrum, as shown in the right figure, where the annual peak is above the significant threshold curve (dashed curve). The two side curves in the wavelet spectrum map indicate the border of the significant region, which lies in the center. The 1-year period of the wavelet power spectrum is then extracted (bottom figure) and calculated for its linear regression trend. Full trend information in 13 continuous stations is given in Table III.

Table V. Decadal and inter-annual variances of eigen maps.

Period →	1955–64	1965–74	1975–84	1985–94	1995–05	1955–05
Eigen map 1 (%)	73.90	71.52	72.20	64.81	65.29	72.27
Eigen map 2 (%)	5.89	5.38	5.76	6.57	5.77	4.55
Eigen map 3 (%)	3.87	4.23	3.10	4.77	3.79	3.08

those of the coastal areas, which explains why the rainfall intensity contrast between the dry and the wet seasons over the mountain areas is higher than that over the coastal area. This contrast comes from the persistent orographic effect during the dry period in the mountain area. This condition explains the previous explanation about the orographic effect in mountain areas and that the coastal area is more susceptible to the annual pattern change.

The first principal component from the EOF method yields yearly variability or the monsoonal pattern that explains about 72% of all variances (the inter-annual data). The analyses of the power density spectrum (Figure 6 right panel) also confirms this result, where it turns out that 1-year is the most dominant period exceeding ten times the others. After the principal component

analyses, we used the PC data for their spectrum analyses through the FFT method and investigated the strength of their components. As we understood before, the most dominant pattern is the annual or monsoonal pattern. In Figure 6 we show the spectrum of the first PC of the decadal dataset. Beside the 1-year period, there is no other clear pattern in lower (above the 1-year period) or higher frequencies (below the 1-year period).

Then, we used the combination of the two methods to detect the climatic trend in the annual signal or the monsoonal dominance. Here, we present two outcomes of applying these methods, i.e. the PC1 power spectrum after applying the FFT method and the variance dominance or percentage. From the FFT power spectrum, we obtain the monsoonal strength of each section or sub-period, as represented by the power density

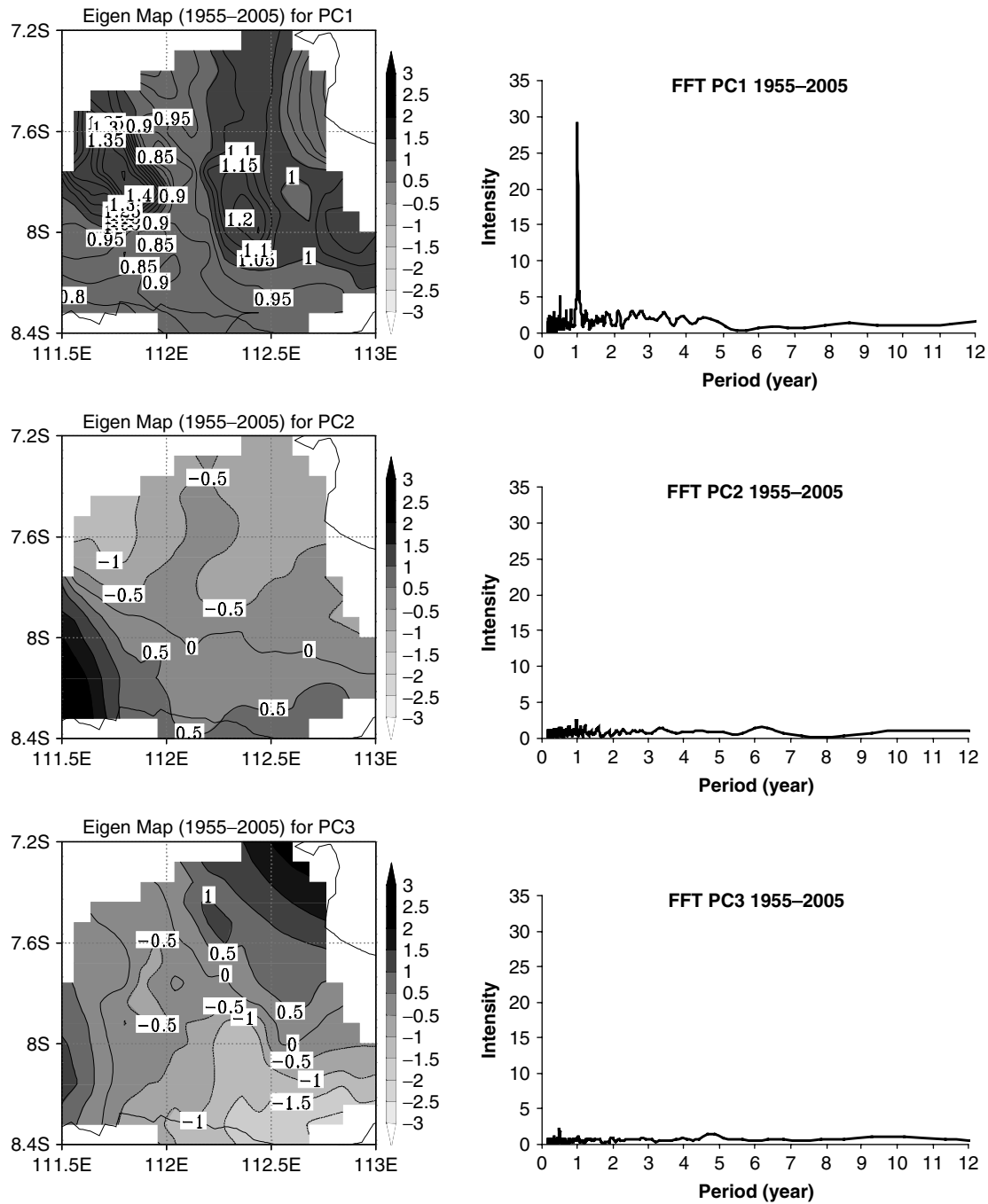


Figure 6. The inter-annual eigen map of PC1, PC2 and PC3 along with their corresponding spectra after FFT. Eigen map 1 has similar positive sign all over, which indicates a homogeneous monsoonal influence, and a strong annual signal. Their respective variances are given in Table IV.

spectrum at the annual frequency. Each sub-period consists of a 10-year time series with a certain central year (Figure 7). We applied the EOF–FFT method for decadal sub-sections and calculated their power density spectra. Hence, changes in this value over time will correspond to changes of the monsoonal strength. The second measure of the monsoonal dominance is in the monsoonal contribution to the whole pattern, or the variance. Since eigen map 1 has a significant annual signal (the monsoonal signal) above the others, we can consider that this eigen map exclusively signifies the monsoonal dominance. Changes of variances from these running eigen

maps in time, therefore, indicate the trend of the monsoonal dominance. In preparing the second approach, we conducted a windowed or running EOF method with the data length of each time series as 10 years starting from 1955 onwards. Thus in total we have about 46 time series. We shall call this method, then, the running EOF variance method. On the contrary, Dai *et al.*, (1997) used directly the second leading EOF as the trend signal for a gridded global precipitation analysis.

The results of applying the combined EOF–FFT method is illustrated in Figure 7, where for reasons of clarity, only decadal values of the power spectrum are

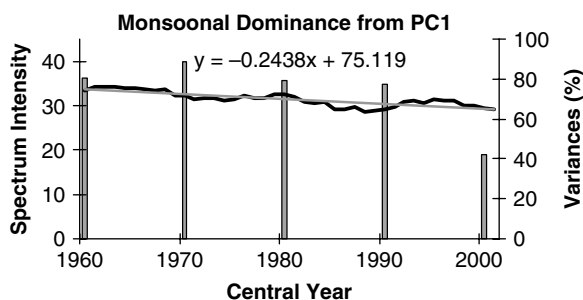


Figure 7. The trend of the monsoonal dominance from power spectra and variances of PC1 from the moving EOF method. Each EOF was performed on a 10-year basis with the central year given in the *x*-axis. The eigen value 1 is considered as monsoonal with a significant annual pattern from its power spectrum. The monsoonal trend is represented here with a declining trend of the power spectrum after FFT (bar graph, left *y*-axis) and the variance percentage of PC1 (line, right *y*-axis). The linear regression trend line (bold straight line) for the variance percentage is given by the formula shown in the graph. The Mann–Kendall trend test *Z*-value for this is -5.79 with a significant level below 0.001.

shown along with smooth running EOF variances of PC1. Although both methods agree on indications of decreasing trends, the variance percentage gives a clearer picture. One disadvantage of the both methods compared to the others (i.e. Mann–Kendall and wavelet) is that the result of EOF–FFT method stands for the whole domain or for no spatial variation. Furthermore, the PC1 power spectrum also suggests a decadal variation of the monsoonal strength. Hence, the strength of the monsoonal pattern over the Brantas catchment is significantly reduced during the last five decades. This conclusion is not clearly seen from the information of the eigen map variances alone but also from the FFT analyses of their PCs.

Following Dai *et al.* (1997), we now examine the temporal and spatial structures of precipitation fields

using EOF analyses (Kutzbach, 1967; Wallace *et al.*, 1993) after removing the annual signal. On the basis of the temporal and spatial patterns of the EOFs, we discuss the likely physical processes behind the leading modes of precipitation fields. The gridded anomalies are first normalized by their standard deviations prior to the EOF analyses. We performed EOF analyses to the leading annual and seasonal modes. The stability of the modes in EOF analyses of subsets of the dataset was also examined with some statistical measures as one of the indications of significance. The time and space components of the first of two leading EOFs (EOF 1) of annual precipitation anomalies are shown in Figure 8. The time component of EOF 1 of annual modes, which accounts for 49.9% of the total variance, replicates the ENSO cycles in the west Equatorial Pacific anomaly sea surface temperature (aSST) in the so-called NINO3 region (150°W – 90°W , 5°S – 5°N) with a correlation value of 0.365 ($p < 0.01$). The correlation value and its significance increase between 1963 and 1982 to about 0.79 ($p < 0.001$). Before and after this period, their correlations decline. Hence, between the Brantas basin rainfall and ENSO there is a quasi-decadal relationship, and the possible ENSO impact for this period is the largest in this area. In fact, ratios of rainfall deviation to aSST deviation in this period are high in comparison to other periods. Another proxy of quasi-decadal ENSO climate variability has been observed from a tree-ring record of central Java (D’Arrigo *et al.*, 2006). The second leading EOF, 8.29% of total variances, exhibits the decadal variability although does not have similar periods as the rainfall ENSO relationship above. This result is different from that of Dai *et al.* (1997), who found the global rainfall trend from the second leading mode of the global EOF pattern. In other regions, The changes in ENSO could not account for the significant

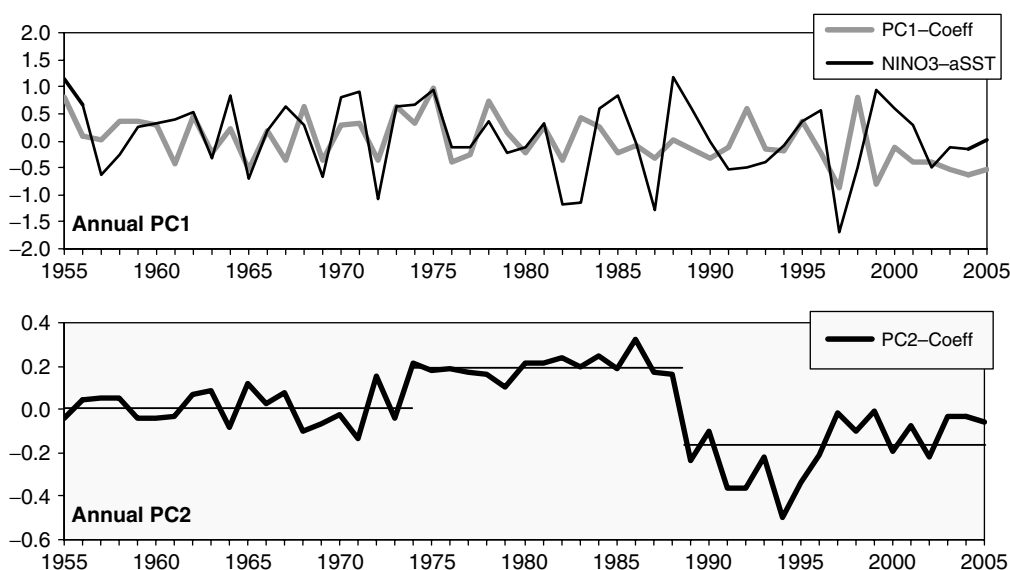


Figure 8. The leading annual eigen coefficients of PC1 and PC2 (black lines) along with the NINO3 aSST (grey lines; in $^{\circ}\text{C}$) for the PC1. For the PC2, the linear straight grey lines highlight the bi-decadal variability at level 0.0, 0.2 and -0.18 during the period 1955–1973, 1974–1988 and 1989–2005, respectively.

decrease over southern Chile, whereas the observed trend in Brazil towards wetter conditions in the southwest and drier conditions in the northeast could be explained by changes in ENSO relationship (Haylock *et al.*, 2006). While the global analysis can capture the most important modes in global precipitation fields, it is likely to miss many regional modes, which is clearly dominant in our analysis. Therefore, this method may not be appropriate in detecting regional climate trend.

EOF analyses of seasonal precipitation revealed that the ENSO signal is present within the first leading EOF in September/October/November (SON) with a significant correlation 0.554 ($p < 0.001$). Less significant signal is present within the JJA leading mode ($p < 0.05$). Like the annual leading mode, the correlation of SON rainfall to aSST increases between 1963 and 1982 to about 0.65 ($p < 0.01$). Aldrian *et al.* (2007) concluded that the SON rainfall over south Indonesia could be used as an ENSO index. As shown in Figure 9, the inter-annual variability of the first leading mode of seasonal precipitation correlates well with the ENSO signal in SON and followed by JJA, while March/April/May (MAM) has the most insignificant correlation owing to the persistent spring barrier (Aldrian *et al.*, 2007 and references therein). Furthermore, this result is in agreement with that of Aldrian and Susanto (2003) for the seasonal correlation strength between Indonesian rainfall and the Equatorial Pacific aSST. The summary of the annual and seasonal leading modes along with their ENSO relationship (by correlation values) is given in Table VI. Note that the variances of anomaly data series are highly correlated to the leading EOF variances. The variances of anomaly data are calculated after normalizing by their standard deviation. Therefore during the peak of the dry period (JJA) with small rainfall amount, the number is large. Comparing between two transition periods, MAM has less variances than SON, which the latter indicating more unstable inter-annual variability. Previously, we also found instability of the second transition period. Here, SON variability is highly sensitive to the ENSO variability, which turns to be the dominant influence for the annual variability as well. Thus, instability of the second transition period mainly comes from the ENSO influence.

Table VI. Variances of leading EOF after removing the annual signal along with their correlations to aSST of NINO3 region and the data series variances. *, **, *** indicate correlation significant to the level of 0.05, 0.01, 0.001, respectively.

	Variances (%)			Correlation PC1 to aSST	Anomaly series variances
	PC1	PC2	PC3		
Annual	49.90	8.29	6.85	** 0.365	0.470
MAM	47.74	8.56	7.18	-0.003	0.455
JJA	73.70	7.45	4.53	* 0.280	0.732
SON	66.60	5.85	5.05	*** 0.554	0.656
DJF	29.16	12.20	9.56	-0.177	0.264

3.4. The seasonal imbalance

After using several analysis methods for detecting the trend, especially the annual trend, we are interested to see what happens to the annual pattern. We already know by both transitional periods, that the first period in the boreal spring is more stable than the one in the boreal fall. From Table III we notice that there is an imbalance between the decreasing trends over the wet season (from October to March) and that over the dry period (from April to September), whereas a larger decreasing trend occurs mostly during the latter. If the rate of decline of the rainfall in the dry season exceeds that of the wet season, then the ratio of rain falls in the wet season to the total and also the number of the dry months (dry spells) will increase.

Actually, there is an increasing trend of the ratio between total rain fall in the wet season to the total annual rainfall, as shown in Figure 10 and in Table VII. Since the inter-annual variabilities are large, with this type of trend detection approach we rarely see a significant trend level. Nevertheless, all stations except, again, Semen have an increasing trend of the ratio. Moreover, there seems to be no relationship on the rate of change in the ratio to the station height, or in other words, there is no role of orography. However, the three largest decreasing trends by m values (the trend's slope) occur in stations below 1000 m. Moreover, as mentioned earlier, the rainfall amount and data variances over the mountainous areas are larger than those over the lowland areas, and therefore a comparable decrease between highland and lowland areas still implies susceptibility of the lowland areas. The increase of the rainfall ratio such as this implies the increasing trend of the dry spell period and the increasing risks of drought in the dry season as well as flood and landslide in the wet season. From Figure 10, we notice that in some years, the whole rain fall during the wet season or have 100% ratio.

On the basis of all the previous explanations, we decided to investigate more on the dry period and compare the condition of rainfall data from two different nearby locations, the mountain area and the coastal areas. For this purpose, we do not derive our comparison on the basis of station data but from the gridded data instead. The mountain area is represented by a grid near Pujon (>1000 m; 112.48°E, 7.81°S), and the coastal area is represented by a grid near the Mojokerto city (<100 m; 112.47°E, 7.37°S). Both stations are located on a similar phase of the eigen map (positive side) and at the northern side of the Kelud and Arjuna (north of Kelud) Mountains. Thus, they will be subjected to similar monsoonal exposure, and no shadowing or Fohn effect will be taken into account. We used a threshold value for an extreme or total dry month of 5 mm/month rainfall in two locations, and the result can be seen in Figure 11. Thus a month with rainfall amount of less than 5 mm/day is assumed as a no rainy day month (extreme dry month).

Mojokerto had more number of extreme dry months, which increased for the last five decades in comparison

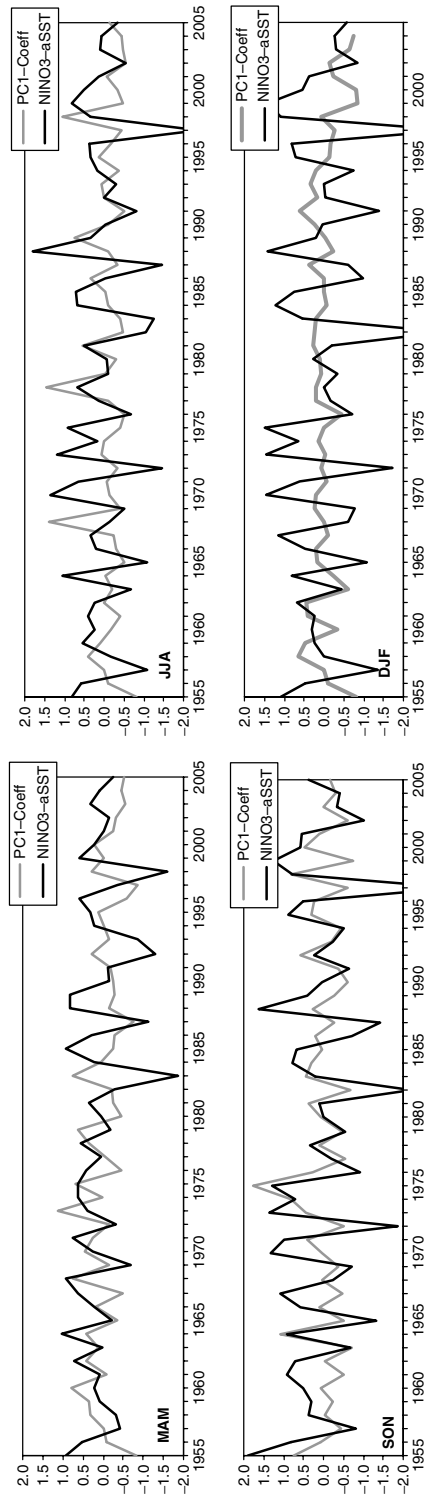


Figure 9. The leading seasonal eigen coefficients of PCI (black lines) after removing the annual signal along with the NINO3 aSST (grey lines; in °C).

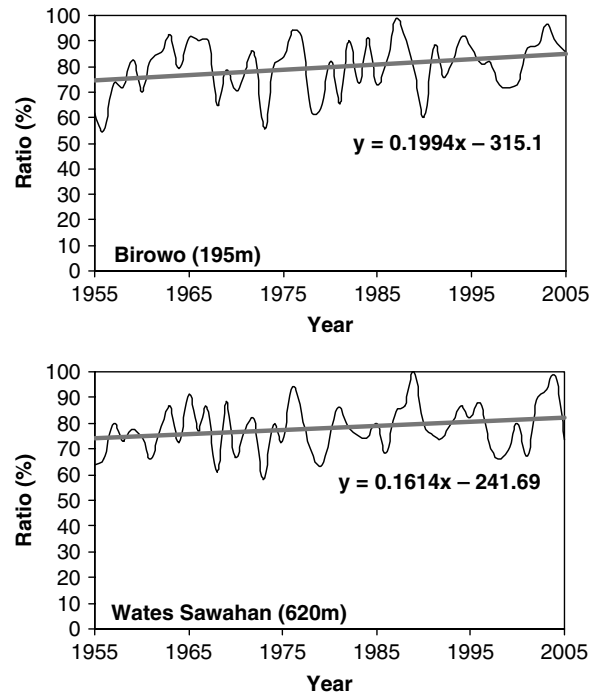


Figure 10. Two examples of increasing trends of ratio of the rainfall in wet season to total annual rainfall during the last five decades.

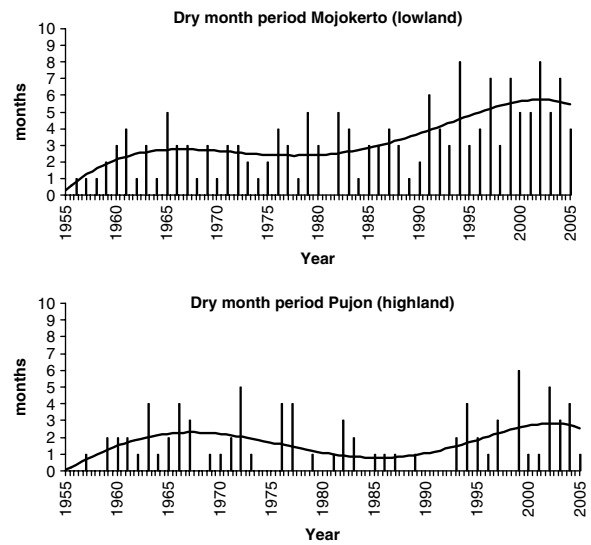


Figure 11. Number of extreme dry months (<5 mm) for Mojokerto (top) and Pujon (bottom) from 1955 to 2005. Curve on each graph is polynomial regression on the fifth power.

to Pujon which is more stable. In the early years of investigation, both had a similar number of dry months, which is about 2 months. However, in the last 10 years the number increased to 4 months and in 2002 it reaches a record of 8 months of dry season, which appears to be the longest dry season for the whole five decades. Meanwhile, the Pujon area has a more stable number of dry months of about 1–2 months for the last 10 years with a maximum of 6 months. This result supports the previous explanation about the orographic rain that occurs in the mountainous area, and reveals that the monsoonal

Table VII. Linear regression of the ratio of rainfall in wet season to total annual from 1955 to 2005 according to the formula: $Percentage\ ratio = m \times year + b$. +, *, **, *** indicate Mann–Kendall significant level of 0.1, 0.05, 0.01, 0.001, respectively.

Station name	Station height (m)	m (%)	b	Mann–Kendall Z	Total changes (%)	Missing data
Tangkil	395	0.13	−1.7571	1.56	6.63	–
Poncokusumo	1120	0.11	−1.4772	1.27	5.61	–
Wagir	1106	0.09	−0.9277	0.79	4.59	–
Birowo	195	0.20	−3.1177	1.67*	10.2	–
Wates Kediri	175	0.12	−1.6341	1.72*	6.12	–
Kediri	70	0.11	−1.3448	1.02	5.61	–
Kertosono	47	0.15	−2.2071	1.53	7.65	–
Tugu	18	0.13	−1.8194	0.93	6.63	–
Dampit	450	0.08	−0.8679	0.81	4.08	1984–1989
Doko	325	0.10	−1.2833	2.14**	5.10	1980–1990
Pujon	1258	0.12	−1.5296	1.78*	6.12	–
Wates Sawahan	620	0.16	−1.4062	1.71*	8.16	–
Semen	625	0.02	0.3997	0.72	1.02	–

negative trend had more effect in the coastal area. As a result, the expansion of the dry area has shifted the balances between the wet season and dry season especially over the lowlands. Thus, the lowland areas are more susceptible to the climate change.

Our results also suggest that the methods employed here are suitable for climatic trend analyses. In this study, we introduced new methods of the use of the annual spectrum of the wavelet and EOF variances to detect the annual trend. The results show that there is no contradiction among methods that we used.

The decrease of the monsoonal strength as detected by the EOF and FFT methods was caused by the imbalances between the wet and dry season that usually lasted about 6 months in the early decade. The annual pattern turns out to be at a different state based on longer dry season in a 1-year period of the monsoon. Longer dry periods with lower rainfall amount may also indicate a global change in the evaporation supply, which has been reduced persistently during the last five decades. Persistent reduction of evaporation may be associated with the global dimming phenomena (Stanhill and Cohen, 2001; Ohmura and Wild, 2002; Liepert, 2002; Roderick and Farquhar, 2002). Long-term and persistent air pollution in the lower and middle atmosphere due to traffic over land, sea and air has reduced the radiation amount received by the surface of the earth. For example, the absorbing aerosols over the Indian subcontinent have led to a statistically significant cooling of about 0.3 °C since the 1970s (Krishnan and Ramanathan, 2002). Air pollutants hinder the solar radiation from reaching the ground. As a result, local evaporation especially over large water bodies will be reduced. The global dimming phenomena may not be the only phenomenon responsible to the reduced evaporation. The critical SST over the Indonesian maritime continent may also be responsible. A higher SST above that critical value does not bring about more evaporation; instead, a higher SST will reduce

it. According to Bony *et al.* (1997a,b), Lau *et al.* (1997) and Aldrian and Susanto (2003) the critical SST during the peak of the wet season or December–January is around 29.6 °C. Complementarily, Walliser and Graham (1993) concluded that at SSTs over 29.5 °C deep atmospheric convection decreases and clouds are no longer formed. If the SST rises above that critical value, then rainfall as well as evaporation will be reduced since more evaporation will take more latent heat away from the sea surface and eventually cool it. The cause of the SST rise comes from the global surface temperature increase or the global warming. However, the increase of the evaporation amount will not occur in the tropics but spill over to the sub-tropics. Analyses of station records have shown that during the last 100 years the globally averaged surface air temperature has increased by $\sim 0.45 \pm 0.15$ °C (Hansen and Lebedeff, 1987, 1988; Vinnikov *et al.*, 1990; Jones and Briffa, 1992; IPCC, 1990, 1992, 1996). The warming is also supported by evidence of increasing water vapour in the troposphere since the mid-1970s in the Tropics (Elliott *et al.*, 1991; Gaffen *et al.*, 1991). Atmospheric thermodynamics suggests that surface warming should increase the surface evaporation and evapotranspiration, all other things being equal. Global dimming and warming have opposite effects, which may lead to the same consequence, i.e. the reduction of local surface evaporation in the tropics, though the explanation and investigation of the probable cause of the evaporation reduction is beyond the scope of this study. As a matter of fact, the global climate change apparently has changed the local climate in this catchment.

4. Concluding remarks

We have investigated and analysed the long-term spatial and temporal variation and trend of climate over the Brantas catchment area, East Java. The analyses

have been performed for the 51-year period (1955–2005) from the monthly rainfall data with several methods: the Mann–Kendall trend test, wavelet, EOF and FFT analyses. We report two major findings in this study. Firstly, there was a significant climatic change temporally and spatially, which resulted in a decrease in the accumulated rainfall monthly and annually. Secondly, we note a decrease of the monsoonal dominance, which leads to changes in the annual pattern and an increase of the rainfall ratio during the wet season and an increase of the dry spell period. Almost all evidences support a decreasing rainfall trend over the catchment area during the recent half century.

The decreasing trend of rainfall in this region is in accordance with the results of Dai *et al.*, 1997, who found that over some parts of the low latitudes (the Philippines, Malaysia, and the Mediterranean), the EOF 2 or the trend signal represents a long-term decrease of precipitation, although globally there is an increase in the precipitation trend, especially in sub-tropical regions. In other tropical regions, Lamb and Peppler (1992) and Nicholson, (1993) have established a declining trend of the sub-Saharan rainfall since the 1950s.

The spatial and temporal climate pattern in the Brantas catchment area is dominated by the monsoonal pattern at a 1-year period. This pattern consequently brings the highest amount of rainfall in DJF, and the lowest in JJA. The local orographic effect regularly happens over the mountains of the Brantas catchment area during the dry season, which preserves the high rainfall area. Hence, the mountainous area is less susceptible to the climatic change. The coastal areas are more influenced by the decrease of the monsoonal strength than the mountain areas, which can be seen by an increase in the number of dry months in recent decades in the coastal area in comparison to the low and a more stable dry period over the mountain areas. In fact, more extensions of the dry areas are detected over the lowland areas.

The climate trend detected by the EOF method shows a decrease of the monsoonal strength in the catchment for the last five decades. This trend is due to the imbalances of the wet and dry seasons, by which the dry season gets longer and spills into the second transitional period (the boreal fall). The ENSO influence on this imbalance is obvious for the second transitional period. The imbalance period brings as a consequence an increasing ratio of rain falls in the wet season to the total annual rainfall and leads to an increased risk of extreme climate condition such as drought over the dry season and flood and landslide over the wet season.

Acknowledgements

This research was partially supported by the SARCS project 94/01/CW and by the INSIDE Project from ASIA Pro ECO-ASI/B7-301/2598/20-2004/79071. Special thanks to Sutopo Purwo Nugroho and the Perum Jasa Tirta I for providing rainfall data.

References

- Aldrian E, Susanto RD. 2003. Identification of three dominant rainfall regions within Indonesia and their relationship to sea surface temperature. *International Journal of Climatology* **23**: 1435–1452.
- Aldrian E, Gates LD, Widodo FH. 2007. Seasonal variability of Indonesian Rainfall in ECHAM4 Simulations and in the Reanalyses: Roles of ENSO. *Theoretical and Applied Climatology* **87**: 41–59.
- Baliunas S, Frick P, Sokoloff D, Soon W. 1997. Time scales and trends in central England temperature data (1659–1990): a wavelet analysis. *Geophysical Research Letters* **24**: 1351–1354.
- Bony S, Lau KM, Sud YC. 1997a. Sea surface temperature and large-scale circulation influences on tropical greenhouse effect and cloud radiative forcing. *Journal of Climate* **10**: 2055–2077.
- Bony S, Sud Y, Lau KM, Susskind J, Saha S. 1997b. Comparison and satellite assessment of NASA/DAO and NCEP-NCAR Reanalysis over tropical ocean: Atmospheric hydrology and radiation. *Journal of Climate* **10**: 1441–1462.
- Braak C. 1921. *Het Climaat van Nederlandsch Indie. Verhandelingen*, vol. 8. Magnetic Meteorology Observation: Batavia.
- Craddock JM. 1979. Methods of comparing annual rainfall records for climatic purposes. *Weather* **34**: 332–346.
- Cressman GP. 1959. An operational objective analysis scheme. *Monthly Weather Review* **117**: 765–783.
- Dai A, Fung IY, DelGenio AD. 1997. Surface observed global land precipitation variations during 1900–88. *Journal of Climate* **10**: 2943–2962.
- D'Arrigo R, Wilson R, Palmer J, Krusic P, Curtis A, Sakulich J, Bijaksana S, Zulaikah S, Ngkoimani LO. 2006. Monsoon drought over Java, Indonesia, during the past two centuries. *Geophysical Research Letters* **33**: L04709.
- Datsenko NM, Shabalova MV, Sonechkin DM. 2001. Seasonality of multidecadal and centennial variability in European temperatures: the wavelet approach. *Journal of Geophysical Research* **116**: 449–463.
- Elliott WP, Smith ME, Angell JK. 1991. Monitoring tropospheric water vapor changes using radiosonde data. *Greenhouse-Gas-Induced Climate Change: A Critical Appraisal of Simulations and Observations*, Schlessinger ME (ed). Elsevier: Amsterdam, The Netherlands; 311–328.
- Gaffen DJ, Barnett TP, Elliott WP. 1991. Space and time scales of global tropospheric moisture. *Journal of Climate* **4**: 989–1008.
- Hackert EC, Hastenrath S. 1986. Mechanisms of Java Rainfall anomalies. *Monthly Weather Review* **114**: 745–757.
- Hansen J, Lebedeff S. 1987. Global trends of measured surface air temperature. *Journal of Geophysical Research* **92**: 13345–13372.
- Hansen J, Lebedeff S. 1988. Global surface air temperatures: Update through 1987. *Geophysical Research Letters* **15**: 323–326.
- Haylock M, McBride JL. 2001. Spatial coherence and predictability of Indonesian wet season rainfall. *Journal of Climate* **14**: 3882–3887.
- Haylock M, Nicholls N. 2000. Trends in extreme rainfall indices for an updated high quality data set for Australia, 1910–1998. *International Journal of Climatology* **20**: 1533–1541.
- Haylock MR, Peterson TC, Alves LM, Ambrizzi T, Anunciação YMT, Baez J, Barros VR, Berlato MA, Bidegain M, Coronel G, Corradi V, Garcia VJ, Grimm AM, Karoly D, Marengo JA, Marino MB, Moncunill DF, Nechet D, Quintana J, Rebello E, Rusticucci M, Santos JL, Trebejo I, Vincent LA. 2006. Trends in total and extreme South American Rainfall in 1960–2000 and Links with sea surface temperature. *Journal of Climate* **19**: 1490–1512.
- IPCC. 1990. *Climate Change, The IPCC Scientific Assessment*, Houghton JT, Jenkins GJ, Ephraums JJ (eds). Cambridge University Press: Cambridge, UK; 364.
- IPCC. 1992. *Climate Change 1992: The Supplementary Report to the IPCC Scientific Assessment*, Houghton JT, Callander BA, Varney SK (eds). Cambridge University Press: Cambridge, UK; 200.
- IPCC. 1996. *Climate Change 1995, The Science of Climate Change*, Houghton JT, Meira Filho LG, Callander BA, Harris N, Kattenberg A, Maskell K (eds). Cambridge University Press: Cambridge, UK; 584.
- IPCC. 2001. *Climate Change. 2001 The Scientific Basis. Contribution of Working Group I to the Third Assessment Report of the Intergovernmental Panel on Climate Change (IPCC)*, Houghton JT, Ding Y, Griggs DJ, Noguer M, Van der Linden PJ, Xiaosu D (eds). Cambridge University Press: Cambridge, UK.
- Jones PD, Briffa KR. 1992. Global surface air temperature variations over the twentieth century: Part I, spatial, temporal and seasonal details. *Holocene* **2**: 165–179.
- Kendall MG. 1938. A new measure of rank correlation. *Biometrika* **30**: 81–93.

- Kendall MG. 1970. *Rank Correlation Methods*. Charles Griffin: London, UK; 272.
- Konnen GP, Jones PD, Kaltofen MH, Allan RJ. 1998. Pre-1866 extensions of the southern oscillation index using early Indonesian and Tahitian meteorological readings. *Journal of Climate* **11**: 2325–2339.
- Krishnan R, Ramanathan V. 2002. Evidence of surface cooling from absorbing aerosols. *Geophysical Research Letters* **29**: 1340.
- Kutzbach JE. 1967. Empirical eigenvectors of sea-level pressure, surface temperature and precipitation complexes over North America. *Journal of Applied Meteorology* **6**: 791–802.
- Lamb PJ, Pepler A. 1992. Further case studies of tropical Atlantic surface atmospheric and oceanic patterns associated with sub-Saharan drought. *Journal of Climate* **5**: 476–488.
- Lau KM, Wu HT, Bony S. 1997. The role of large-scale atmospheric circulation in the relationship between tropical convection and sea surface temperature. *Journal of Climate* **10**: 381–392.
- Liepert B. 2002. Observed reductions of surface solar radiation at sites in the US and Worldwide. *Geophysical Research Letters* **29**: 1421–1433.
- Mann HB. 1945. Non-parametric test of randomness against trend. *Econometrica* **13**: 245–259.
- Manton MJ, Della-Marta PM, Haylock MR, Hennessey KJ, Nicholls N, Chambers LE, Collins DA, Daw G, Finet A, Gunawan D, Inape K, Isobe H, Kestin TS, Lefale P, Leyu CH, Lwini T, Maitrepierre L, Ouprasitwong N, Page CM, Pahalad J, Plummer N, Salinger MJ, Suppiah R, Tran VL, Trewin B, Tibig I, Yee D. 2001. Trends in extreme daily rainfall and temperature in southeast Asia and the South Pacific: 1961–1998. *International Journal of Climatology* **21**: 269–284.
- Nicholson SE. 1993. An overview of African rainfall fluctuations of the last decade. *Journal of Climate* **6**: 1463–1466.
- Ohmura A, Wild M. 2002. Climate change: Is the hydrological cycle accelerating? *Science* **298**: 1345–1346.
- Park J, Mann ME. 2000. Interannual temperature events and shifts in global temperature: a multiple wavelet correlation approach. *Earth Interactions* **4-1**: 1–53.
- Peterson TC, Easterling DR, Karl TR, Groisman P, Nicholls N, Plummer N, Torok S, Auer I, Boehm R, Gullett D, Vincent L, Heino R, Tuomenvirta H, Mestre O, Szentimrey TS, Salinger J, Førland EJ, Hanssen-Bauer I, Alexandersson H, Jones P, Parker D. 1998. Homogeneity adjustments of In Situ atmospheric climate data: A review. *International Journal of Climatology* **18**: 1493–1517.
- Pisoft P, Kalvová J, Brázdil R. 2004. Cycles and trends in the Czech temperature series using wavelet transforms. *International Journal of Climatology* **24**: 1661–1670.
- Preisendorfer RW. 1988. *Principal Component Analysis in Meteorology and Oceanography*. Elsevier Science: New York; 425.
- Press WH, Rybicki GB. 1989. Fast algorithm for spectral analysis of unevenly sampled data. *The Astrophysical Journal* **338**: 277–280.
- Roderick M, Farquhar G. 2002. The cause of decreased pan evaporation over the past 50 years. *Science* **298**: 1410–1411.
- Stanhill G, Cohen S. 2001. Global dimming: A review of the evidence. *Agricultural and Forest Meteorology* **107**: 255–278.
- Suppiah R, Hennessey KJ. 1998. Trends in total rainfall, heavy rain events and numbers of dry days in Australia. *International Journal of Climatology* **18**: 1141–1164.
- Torrence C, Compo GP. 1998. A practical guide to wavelet analysis. *Bulletin of American Meteorological Society* **79**: 61–78.
- Vinnikov KY, Groisman PY, Lugina KM. 1990. Empirical data on contemporary global climate changes (temperature and precipitation). *Journal of Climate* **3**: 662–677.
- von Storch H. 1995. Spatial patterns: EOFs and CCA. In *Analysis of Climate Variability. Application of Statistical Techniques*, von Storch H, Navarra A (eds). Springer: Berlin, Heidelberg; 227–258.
- Wallace JM, Zhang Y, Lau KH. 1993. Structure and seasonality of interannual and interdecadal variability of the geopotential height and temperature fields in the Northern Hemisphere troposphere. *Journal of Climate* **6**: 2063–2082.
- Walliser DE, Graham NE. 1993. Convective cloud systems and Warm-Pool sea surface temperatures: coupled interactions and self regulation. *Journal of Geophysical Research* **98**: 12881–12893.
- Wilks SD. 1995. *Statistical Methods in the Atmospheric Sciences*. *International Geophysics Series*, 59. Academic Press: Burlington, MA, USA. 467.